Acta Oceanol. Sin., 2015, Vol. 34, No. 9, P. 35–42
DOI: 10.1007/s13131-015-0734-4
http://www.hyxb.org.cn
E-mail: hyxbe@263.net

Shoaling of the internal solitary waves over the continental shelf of the northern South China Sea

QIAN Hongbao[1, 2], HUANG Xiaodong[1]*, TIAN Jiwei[1], ZHAO Wei[1]

[1] Physical Oceanography Laboratory, Ocean University of China, Qingdao 266100, China

[2] The Administrative Centre for China's Agenda 21, Beijing 100089, China

Received 23 November 2014; accepted 12 February 2015

Abstract

The activities of internal solitary waves (ISWs) over the continental shelf of the northern South China Sea (SCS) are of high complexity. In this study, we investigated the spatial-temporal characteristics of the shoaling ISWs over the northern SCS continental shelf using the satellite images and the results of numerical simulation. The examination of the ISW signals in the satellite optical images revealed the existence of three types of ISWs in the region north to the Dongsha Island, namely, mode-1 depression ISW, mode-1 elevation ISW, and mode-2 convex ISW. The geographical distributions of these ISWs were derived from the satellite images. Numerical results exhibited the process of polarity conversion of ISWs, by which mode-1 elevation waves were transformed from the shoaling mode-1 depression waves. The mode-2 convex ISWs generally followed the mode-1 depression ISWs. The numerical results suggested that the interaction of the mode-1 depression ISWs with the up-slope topography locally generated mode-2 ISWs, and such waves of high vertical mode dissipated rapidly during the inshore propagation.

Key words: internal solitary wave, nonlinear internal wave, South China Sea, vertical mode

Citation: Qian Hongbao, Huang Xiaodong, Tian Jiwei, Zhao Wei. 2015. Shoaling of the internal solitary waves over the continental shelf of the northern South China Sea. Acta Oceanologica Sinica, 34(9): 35–42, doi: 10.1007/s13131-015-0734-4

1 Introduction

Internal solitary waves (ISWs) with large amplitudes and high frequencies have been frequently observed in global oceans. They are especially active on the coastal shelves (Haury et al., 1979; Moum et al., 2007; Stanton and Ostrovsky, 1998) and in marginal seas (Apel et al., 1985; Osborne and Burch, 1980). The ISWs in the northern South China Sea (SCS) have attracted particular attention of oceanographers. The reasons for this interest are related both to their large amplitudes (Buijsman et al., 2012) and to their large spatial coverage (Zhao et al., 2004). Recent studies showed that the ISWs played an important role in the enhanced turbulence (St Laurent et al., 2011) and the vertical transport of material (Moore and Lien, 2007) in the northern SCS.

The Luzon Strait (LS), with a north-south width of approximately 365 km, is the major passage connecting the SCS to the western Pacific Ocean. It owns a double submarine ridge system. The strong barotropic tidal current flowing over these two ridges produces a large amount of internal tides into the northern SCS and the western Pacific Ocean (Jan et al., 2008). Previous studies suggested that the internal tides entering to the northern SCS gave rise to large-amplitude depression solitary waves through the nonlinear steepening mechanism (Farmer et al., 2009; Helfrich and Grimshaw, 2008; Li and Farmer, 2011; Zhao et al., 2004). These ISWs were generally considered to be mode-1 ISWs, because they forced the isopycnals in the whole depth move upward/downward uniformly. A thorough review and reference list of the mode-1 ISWs in the SCS can be found in Cai et al. (2012). In the deep water with little change in the bottom topography, these mode-1 ISWs owned the ability of propagating with nearly unchanged waveforms and at nearly constant speeds (Klymak et al., 2006), as a result of the balance between the nonlinear and nonhydrostatic dispersion effects.

However, as propagating onto the continental shelf, the background conditions in which the mode-1 ISWs evolve vary significantly owing to the changes of the topography. Since the decrease of the bottom depth tends to amplify the nonlinearity and reduce the nonhydrostatic dispersion effect of the ISWs, their wave patterns steepen and widths become narrower (Alford et al., 2010). Those authors also demonstrated that the shoaling of the bottom depth caused the propagation speeds of mode-1 ISWs to drop from 3–4 m/s in the deep water to around 1.5 m/s over the continental shelf slope. For the large-amplitude mode-1 ISW, its maximum orbital current of 2 m/s would exceed its propagation speed, which led to the breaking of the ISW and formed one trapped core with a turbulent kinetic energy dissipation of $O(10^{-4})$ (W/kg) (Lien et al., 2012). Along the propagation direction of the ISWs, the shoaling of the bottom depth results in the reducing of the lower layer thickness, while the upper layer thickness remains to be constant. As encountering the critical depth where the thickness of the lower layer equals to the upper layer, the polarity conversion process will occur, by which the mode-1 depression ISWs will be converted into mode-1 elevation ISWs.

Foundation item: The National Key Basic Research Program (973 Program) of China under contract No. 2014CB745003; the National High Technology Research and Development Program (863 Program) of China under contract No. 2013AA09A502; the Key Laboratory of Physical Oceanography of MOE under contract No. 201413032; the National Key Scientific Research Project "The South China Sea Deep" under contract No. 91028008; the National Natural Science Foundation of China under contract Nos 41176008 and 41176010.

*Corresponding author, E-mail: xhuang@ouc.edu.cn

Zhao et al. (2003) and Orr and Mignerey (2003) investigated the polarity conversion process of the mode-1 ISWs over the continental shelf of the northern SCS on the basis of satellite images and field observations, respectively.

During the passage of the mode-2 ISWs, isotherms displacements in the upper and lower layer are out of phase. Compared to the mode-1 ISWs, there is less opportunity to capture mode-2 ISWs in the ocean. Recent observational study over the continental shelf of the northern SCS has revealed the occurrences of the mode-2 ISWs, which were occasional in summer and frequent in summer (Yang et al., 2009). Both of the convex and concave mode-2 ISWs were observed in the shallow water, which one to occur depended on the thickness of the middle layer (Yang et al., 2010). Based on fully nonlinear simulation, Chen et al. (2014) systematically examined the dependence of the generation of the mode-2 internal tides and their nonlinear disintegration into mode-2 ISWs on the density stratification, and suggested that a deeper pycnocline with a thickness of 80 m is favorable for the formation of the mode-2 ISWs.

Due to the limited field observations, the understanding of the shoaling process of the ISWs over the continental shelf of the northern SCS is still poor. In this study, making use of Moderate Resolution Imaging Spectroradiometer (MODIS) images, we qualitatively analyzed the surface features of ISWs with different polarities and vertical modes and attempted to obtain their geographical distributions. Based on the numerical modeling, we examined the shoaling process of depression ISWs over the upslope topography of the continental shelf. The paper is organized as follows. Section 2 provides the analysis of the surface expressions of ISWs in the MODIS images. Section 3 gives the analysis of the results of numerical simulation. The final section provides the conclusions of this study.

2 Satellite observation

2.1 *ISWs in the two MODIS images*

In this study, we focused on the ISW activities in the region north to the Dongsha Island as marked by the rectangle in Fig. 1, where the topography is featured by a westward shoaling from 1 000 m to 100 m. Two MODIS optical images (Fig. 2) covering the study region were acquired on August 20 and 21, 2011, respectively, with a resolution of 250 m. The ISWs appear as alternating bright/dark stripes, and most of them contain a group of solitary waves, denoting multi-wave ISW packets. One can see that there were five groups of ISWs in the image on August 20, which were named as waves *E*–*I* for convenience. In the image of the next day, the waves *H* and *I* were observed again. Comparisons between the two images show that the wave *I* disintegrates into a number of solitary waves after entering the slope region. On average, the south part of the wave *I* propagates at a speed of 1.72 m/s, while its north part propagates at a speed of 1.26 m/s. Such meridonal nonuniformity results in the ISWs with curved crest lines in the shallow water. At the same time, a locally generated wave *H1* emerge between the waves *H* and *I*, and a trans-basin ISWs *J* entered to the image from the east lateral boundary.

Through examining the sea surface manifestations of ISWs, we found that there existed several kinds of ISWs over the continental shelf. The black rectangles in Fig. 2 mark four ISW segments with patterns of dark-light stripes, dark-light-dark stripes, light-dark stripes, and light-dark stripes, respectively. Inside the sunlit regions in the MODIS images, the convergence regions induced by these ISWs appear as dark stripes, while the divergence regions appear as light strips (Mitnik et al., 2000), which is exactly the opposite of what the ISWs do in the SAR images. To clearly show the spatial structures of the ISWs, we extracted the value of gray level of the satellite images along the sections perpendicular to the wave crest lines, as shown in Fig. 3. The ISW in the rectangle R1 with the dark-light stripes leads to one low and one peak in the value of gray level, indicating a convergence region in the wave front and a divergence region in the wave rear, respectively. The measured value of gray level in the rectangle R2 shows variations with a sandwiched structure consisting of one peak and two lows, suggesting that there exist convergence, divergence, and convergence regions from the wave front to wave rear. For the ISWs in the rectangles R3 and R4, the variations in the value of the gray level suggest that the waves have a divergence region in the wave front and a convergence region in the wave rear, respectively, contrary to the ISW event in the rectangle R1.

Figure 2 shows that the incident ISWs from the deep basin

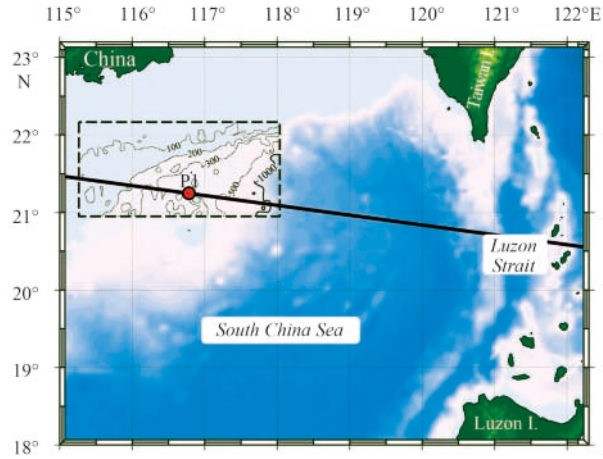

Fig. 1. The topography of the northern South China Sea and the Luzon Strait. The rectangle in dashed lines indicates the focused area of this study. The bold line shows the propagation track of the ISWs assumed in the numerical simulation.

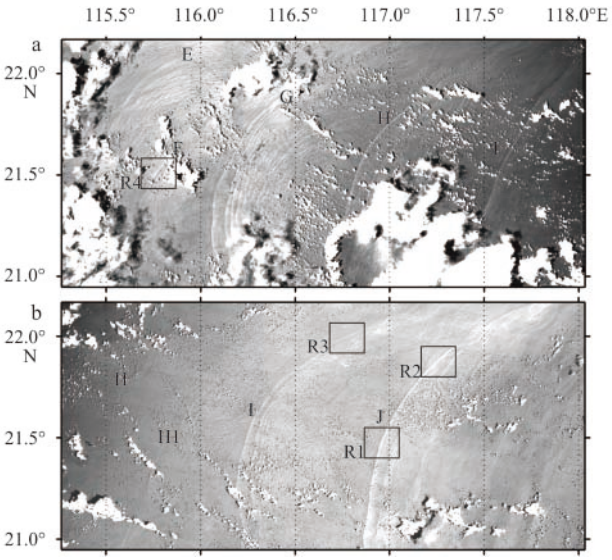

Fig. 2. The MODIS image covering the northern SCS continental shelf acquired on UTC time 20 August 2011 05:25:00 (a) and 21 August 2011 03:00:00 (b).

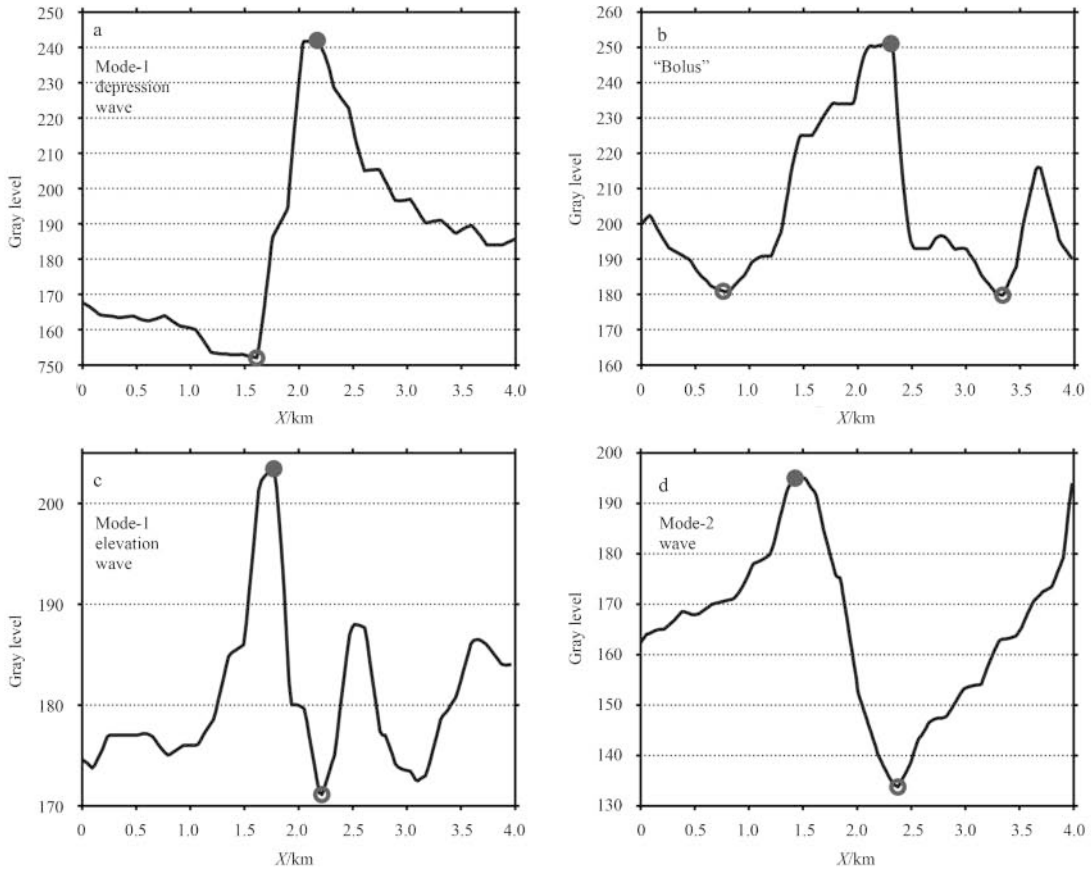

Fig. 3. The gray level of the MODIS image along the sections perpendicular to the crest lines of ISWs inside the rectangle R1 (a), R2 (b), R3 (c) and R4 (d) in Fig. 2.

generally appear as dark-light stripes like the ISW in the rectangle R1, characteristics of which suggest that they are mode-1 depression ISWs. After propagating onto the continental shelf, the north part of mode-1 depression ISWs manifest as dark-light-dark stripes as approaching the area of R2, and in the next stage of the evolution they appear as light-dark stripes in the area of R3 contrary to their surface expressions in R1. In fact, these two stages comprise the polarity conversion process of the ISWs, by which the mode-1 elevation ISWs were transformed from the mode-1 depression ISW (Zhao et al., 2003). The analytical analysis in Section 2.2 shows that polarity conversion processes occur at the critical depth where the nonlinear coefficient α_1=0. Meanwhile, the south part of the incident mode-1 depression ISW experiences a shoaling topography with a less steepness than its north part. Mode-2 convex ISWs, with sea surface features as shown in the rectangle R4, locate around the 21.5°N and follow the mode-1 depression ISWs. The numerical study suggests that they are generated by the interaction of the mode-1 depression ISWs with the up-slope topography, as will be shown in Section 3.

2.2 *Analytical analysis*

The solitary wave will maintain a constant and stable shape as it travels over an unchanged topography because of the balance between nonhydrostatic dispersion and nonlinearity effects. The KdV equation that describes weakly nonlinear internal waves is given as follows:

$$\frac{\partial \eta}{\partial t} + c_0 \left(\frac{\partial \eta}{\partial x} + \gamma \frac{\partial^3 \mu}{\partial x^3} + \alpha \eta \frac{\partial \eta}{\partial x} \right) = 0. \tag{1}$$

Here, η is the wave shape, c_0 is the linear internal wave speed, α is the nonlinear coefficient and β is the nonhydrostatic dispersion coefficient. They can be determined using the following formulas (Lee and Beardsley, 1974):

$$\begin{aligned} \alpha &= \frac{3}{2} \int_{-H}^{0} \rho_0(z) (f_n')^3 \, \mathrm{d}z \Big/ \int_{-H}^{0} \rho_0(z) (f_n')^2 \, \mathrm{d}z, \\ \gamma &= \frac{1}{2} \int_{-H}^{0} \rho_0(z) (f_n)^2 \, \mathrm{d}z \Big/ \int_{-H}^{0} \rho_0(z) (f_n')^2 \, \mathrm{d}z, \end{aligned} \tag{2}$$

in which f is the eigenfunction, n means the vertical mode, and the prime denotes the vertical differentiation. The eigenfunction f can be solved by the boundary value problem (Apel et al., 2007):

$$\frac{d}{z} \left[\rho_0(z) \frac{\mathrm{d}f_n}{\mathrm{d}z} \right] + \rho_0(z) \frac{N^2(z)}{c_n^2} f_n = 0, \tag{3}$$

$$f_n(z) = 0, z = 0, \tag{4}$$

$$f_n(z) = 0, z = -H, \tag{5}$$

where H is the water depth, ρ_0 is the density, and N is the Brunt-Väisälä frequency.

To qualitatively analyze the shoaling process of the ISWs, we obtained the spatial distribution of the mode-1 nonlinear coefficient α_1 using the World Ocean Atlas 2001 (WOA01) data, as shown in Fig. 4b. The results show that the positive α_1 at which the upper layer is thicker than the lower layer is mainly present around the 22°N, consistent with the region where the mode-1 el-

evation ISWs appear in the MODIS images of Fig. 2. With the negative α_1 value, the stratification in the water deeper than 160 m is characterized by the thicker lower layer than the upper layer, where the ocean environment is suitable for the propagation of the mode-1 depreesion wave, in agreement with the satellite observations.

3 Numerical experiment

The ISW activies in the satellite images suggest that the evolution process of ISWs over the continental shelf of the northern SCS is complicated. To reproduce the shoaling process of the ISWs and gain a better understanding on the wave dynamics contained therein, we performed a numerical simulation using the Massachusetts Institute of Technology general circulation model (MITgcm) (Marshall et al., 1997), which is a fully nonhydrostatic model rooted in the incompressible Navier-Stokes equations, and is suitable in simulating the smallest scale motions such as ISWs in the ocean.

3.1 *Model setup*

A bathymetry, along the section from the LS to the continental shelf as the dotted line in Fig. 1 shows, was extracted from ETOPO1 (Fig. 5a) and used in the simulation. The computation domain had 1 832 grids in horizontal with spacing of 500 m. A 10 m vertical grid spacing was adopted in the upper 300 m and it increased in a hyperbolic tangent function form to 100 m at the depth of 4 100 m. A sponge zone of 50 grid points was imposed in the lateral boundaries to absorb energy of baroclinic internal waves and to prevent the reflection of ISWs.

The salinity and temperature field in the simulation were started with the spatially averaged WOA01 summer data in the northern SCS. Tidal elevation and current forcing were applied using the Flather open boundary conditions (Flather, 1976), as shown in Fig. 6. The information of the surface tides were extracted from the global ocean barotropic tide model TPXO 7.2 in the astronomical tide constituents. In the numerical experiments, Coriolis parameter f was set to 5.2×10^{-5} rad/s, corresponding to

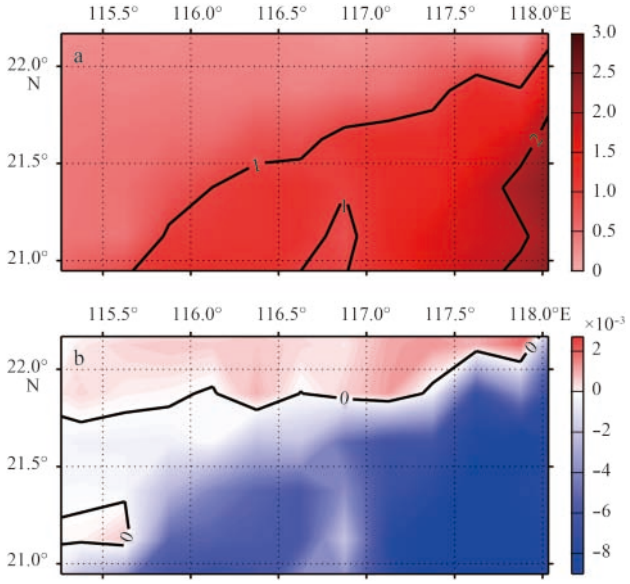

Fig. 4. The mode-1 linear phase speed (m/s) (a) and the mode-1 nonlinear coefficient (b) over the continental shelf of the northern SCS.

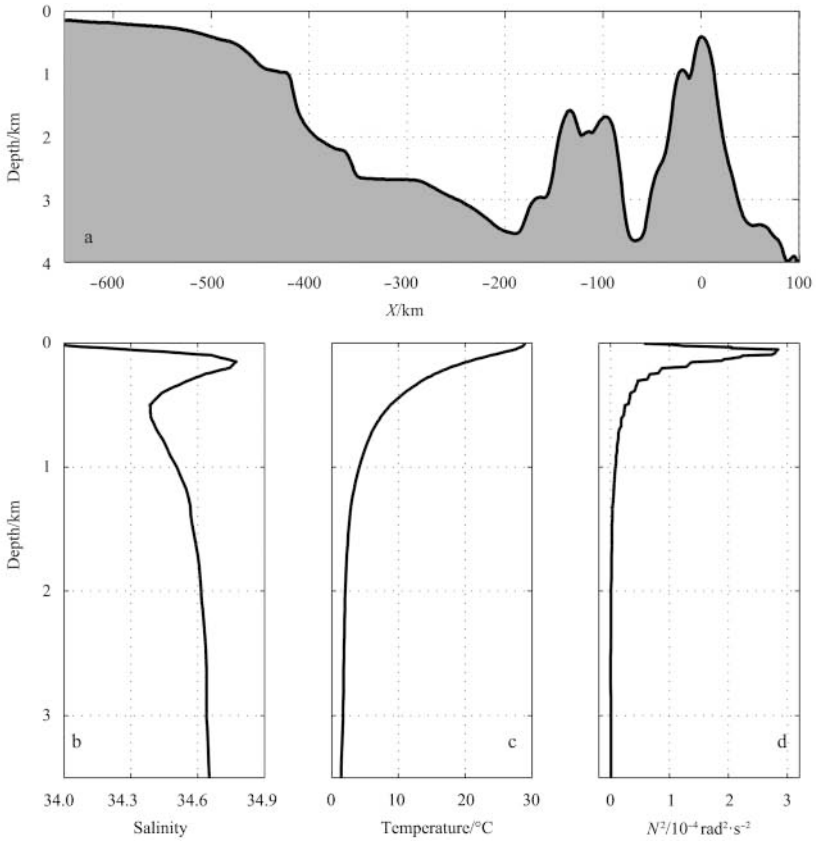

Fig. 5. Bathymetry (a), salinity (b), potential temperature (c), and Brunt–Väisälä frequency (d) used in the numerical simulation.

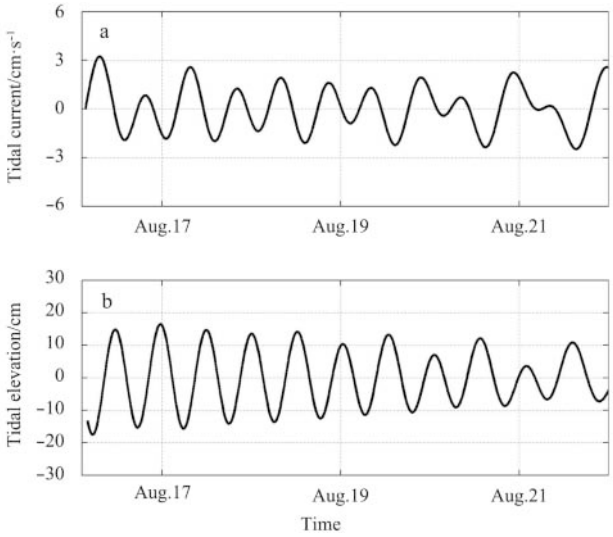

Fig. 6. The tidal forcing imposed at the open boundary. a. Tidal current and b. tidal elevation.

the latitudinal location of the northern SCS at 21°N. The background horizontal diffusivity and viscosity were 10^{-3} m^2/s, and the background vertical diffusivity and viscosity were 10^{-5} m^2/s.

3.2 *Numerical results*

The simulated temperature and velocity field at the site P1 (Fig. 1), where the crest line of the ISW *H* in the MODIS image (Fig. 2a) intersected the bold line in Fig. 1, were extracted and examined (Fig. 7). Similar to the observational results of the moorings (Buijsman et al., 2012; Ramp et al., 2004), there were two ISW occurrences in each day. The ISW *H* arrived at P1 on 20 August 2011 05:33, which was quite close to the time (05:25) when it emerged in the MODIS image. Thus, our numerical results seem to have reliable bases for analyzing the shoaling process of the ISWs over the continental shelf.

Figure 8 presents a series of snapshots of the temperature field that captured the shoaling process of the mode-1 depression ISW over the northern SCS continental shelf. The topography that the ISWs encountered was featured by a spatially-averaged slope of 0.001 4. Totally five ISWs radiating out from the LS travelled across the deep basin and approached the continental shelf within the experimental period of 60 h. The first incident depression ISW have an amplitude of 80 m at the depth of 160 m as entering the shelf region (by the time of 0 h), and this ISW had appeared as a wavetrain by the time of 15 h due to the fission of wave. In the following analysis, the shoaling evolution of the leading wave in the wavetrain is focused (marked by the black arrows in Fig. 8). During the inshore propagation, the front face of the ISW flattened while the rear face of it steepened (by the time of 30 h), owing to that the propagation speed of the trough of the ISW was lowest. By the time of 45 h, a mode-1 elevation ISW had been formed at the wave rear at the place where the bottom depth was around 160 m. Note that the leading depression wave still coexisted with the elevation wave at this moment, and thus they manifest as dark-light-dark stripes within the sunlit region of the MODIS image, e.g., in Fig. 3b. The next stage of the evolution of this ISW was characterized by the continuous flattening of the front face of the leading depression wave. By the time of 60 h, the leading depression wave had been almost diminished. Only the elevation waves could propagated into the region with bottom depth shallower than 100 m, and it appeared as light-dark stripes within the sunlit region of the MODIS image, as shown in Fig. 3c.

On the other hand, a number of mode-2 ISWs were observed over the continental shelf in the numerical simulation, which

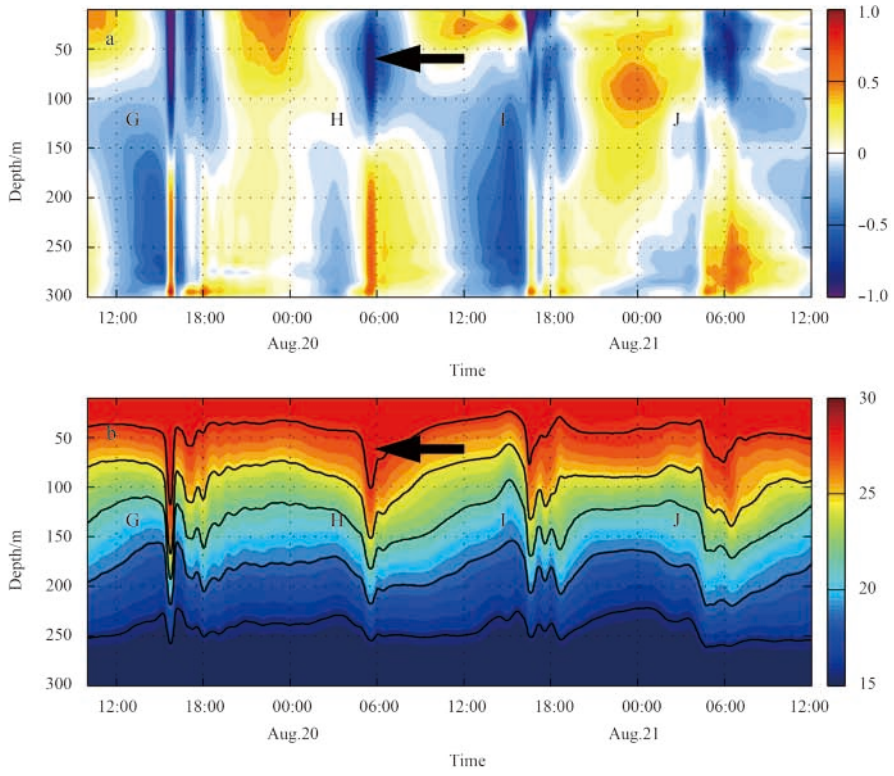

Fig. 7. The simulated velocity (a) (cm/s) and temperature (b) (°C) field at Site P1 in Fig. 1, where the black arrows denote the ISW *H* in the MODIS images (Fig. 2).

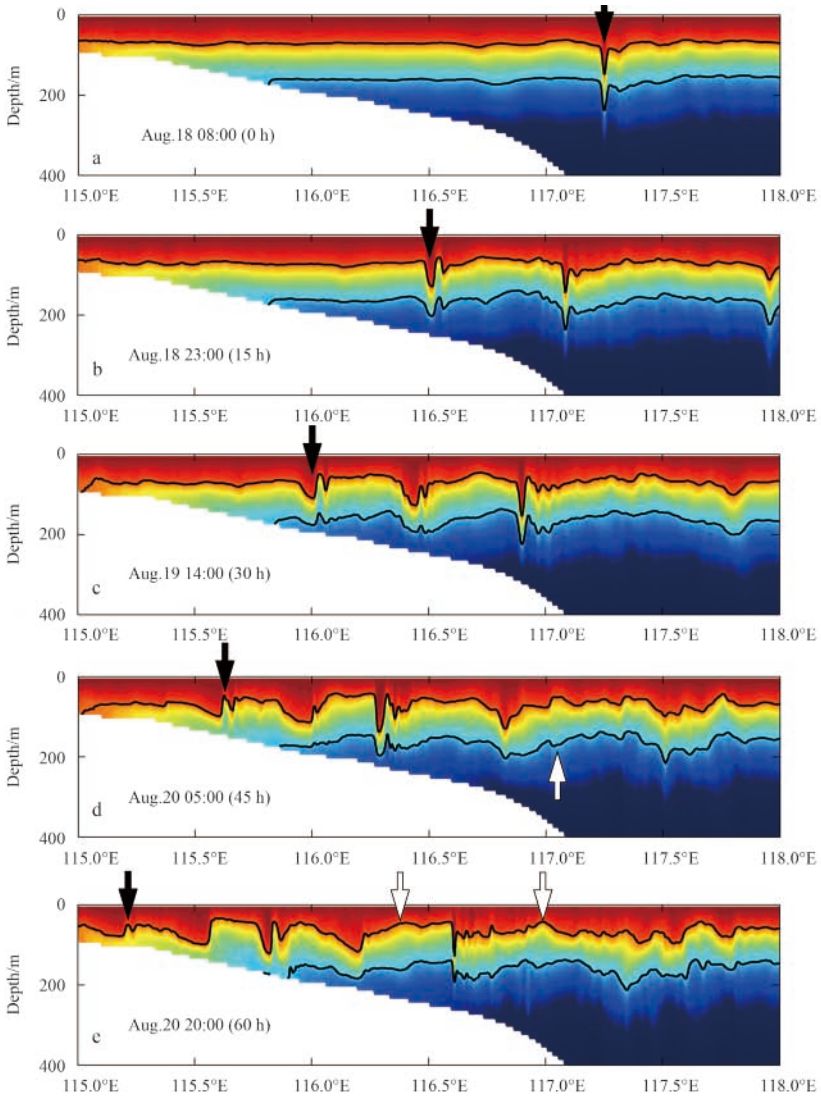

Fig. 8. The results of a numerical simulation showing the changes of the temperature field induced by the shoaling of depression ISWs radiating out from the LS. The black arrows mark the location of the first ISW in the simulation, and the white arrows mark the mode-2 ISW episodes.

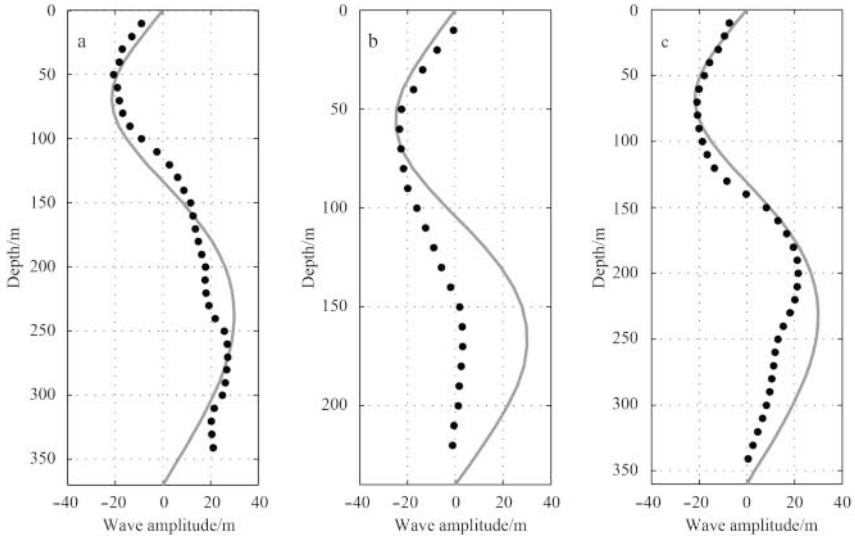

Fig. 9. The isotherm displacements at the crest of the ISWs marked by white arrows in Fig. 8. Black dots: the calculation results of the simulation; and gray curves: theoretical results through solving the boundary value problem.

displaced the isopycnals above and below the thermocline out of phase, as the white arrows in Fig. 8 mark. We calculated the isotherm displacements at the crest of these ISWs (Fig. 9). Based on the simulated stratification, we computed the theoretical vertical structure of the mode-2 internal waves through solving the boundary value problem (Eq. (4)). The comparisons (Fig. 9) reveal that the variations of simulated isopycnal displacements are in good agreement with theoretical mode-2 vertical structure. With a "double-humped" waveform as the white arrows in Fig. 8 mark, we referred to these waves as mode-2 convex ISWs following Yang et al. (2010). One common feature of the reproduced mode-2 waves was that they generally followed the large-amplitude mode-1 depression ISWs. No evidence for the incoming mode-2 ISWs from the deep water was seen in the numerical results, suggesting that they were locally created by the mode-1 depression ISWs as encountering the up-slope topography. All of the mode-2 ISWs existed in the slope region where the bottom depth was 200 to 400 m. Moreover, the numerical simulation suggested that the mode-2 ISWs dissipated rapidly during the propagation, and thus they were less frequently observed in the field experiment. In the MODIS image as shown in Fig. 2, the mode-2 ISWs (waves F and H1) seemed to appear around 21.5°N, with much shorter crest line lengths (20–30 km) than the preceding mode-1 ISWs. The water depth there is around 200 m, in agreement with the numerical results.

4 Conclusions

Making use of the MODIS images, we observed a variety of ISWs with different polarities and modes that existed over the continental shelf of the northern SCS, including mode-1 depression ISWs, mode-1 elevation ISWs and mode-2 convex ISWs. The geographical distributions of these kinds of ISWs were obtained. The mode-1 depression ISWs were widely spread in the region where the bottom depth was deeper than 160 m. Analytical analysis based on the solutions of the KdV equation suggested that the ocean stratification within the region around the 22°N favored the occurrences of polarity conversion process of the ISWs, by which the mode-1 depression ISW changed into the ISW of elevation. By utilizing the MITgcm, the evolution process of the depression ISWs shoaling over the continental shelf slope were examined, and the spatial-temporal characteristics of the shoaling ISWs were given. The polarity conversion process of ISWs reproduced by the numerical simulation was in good qualitative agreement with the satellite observation. The results of the numerical simulation suggest that the mode-2 convex ISWs were produced locally by the interaction of the mode-1 depression ISWs with the up-slope topography, and that the lifetime of the mode-2 ISWs were transient owing to the rapid dissipation. Field observations are needed to quantitatively describe the mixing and dissipation processes of the ISWs during the inshore propagation.

Acknowledgements

The MODIS data used in the study are available online at http://ladsweb.nascom.nasa.gov/.

References

Alford M H, Lien R -C, Simmons H, et al. 2010. Speed and evolution of nonlinear internal waves transiting the South China Sea. Journal of Physical Oceanography, 40(6): 1338–1355

Apel J R, Holbrook J R, Liu A K, et al. 1985. The Sulu Sea internal soliton experiment. Journal of Physical Oceanography, 15(12): 1625–1651

Apel J R, Ostrovsky L A, Stepanyants Y A, et al. 2007. Internal solitons in the ocean and their effect on underwater sound. Acoustical Society of America Journal, 121(2): 695

Buijsman M C, Uchiyama Y, McWilliams J C, et al. 2012. Modeling semidiurnal internal tide variability in the Southern California Bight. Journal of Physical Oceanography, 42(1): 62–77

Cai Shuqun, Xie Jieshuo, He Jianling. 2012. An overview of internal solitary waves in the South China Sea. Surveys in Geophysics, 33(5): 927–943

Chen Zhiwu, Xie Jieshuo, Wang Dongxiao, et al. 2014. Density stratification influences on generation of different modes internal solitary waves. Journal of Geophysical Research: Oceans, 119(10): 7029–7046

Farmer D, Li Qiang, Park J-H. 2009. Internal wave observations in the South China Sea: The role of rotation and non-linearity. Atmosphere-Ocean, 47(4): 267–280

Flather R A. 1976. A tidal model of the north-west European continental shelf. Mem Soc Roy Sci Liege, Ser 6, 10: 141–164

Haury L R, Briscoe M G, Orr M H. 1979. Tidally generated internal wave packets in Massachusetts Bay. Nature, 278(5702): 312–317

Helfrich K R, Grimshaw R H J. 2008. Nonlinear disintegration of the internal tide. Journal of Physical Oceanography, 38(3): 686–701

Jan S, Lien R-C, Ting Chihua. 2008. Numerical study of baroclinic tides in Luzon Strait. Journal of Oceanography, 64(5): 789–802

Klymak J M, Pinkel R, Liu C-T, et al. 2006. Prototypical solitons in the South China Sea. Geophysical Research Letters, 33(11): L11607

Lee Chiyuan, Beardsley R C. 1974. The generation of long nonlinear internal waves in a eeakly stratified shear flow. J Geophys Res, 79(3): 453–462

Li Qiang, Farmer D M. 2011. The generation and evolution of nonlinear internal waves in the deep basin of the South China Sea. Journal of Physical Oceanography, 41(7): 1345–1363

Lien R-C, D'Asaro E A, Henyey F, et al. 2012. Trapped core formation within a shoaling nonlinear internal wave. Journal of Physical Oceanography, 42(4): 511–525

Marshall J, Adcroft A, Hill C, et al. 1997. A finite-volume, incompressible Navier Stokes model for studies of the ocean on parallel computers. J Geophys Res, 102(C3): 5753–5766

Mitnik L, Alpers W, Chen K S, et al. 2000. Manifestation of internal solitary waves on ERS SAR and SPOT images: similarities and differences. In: Proceedings of the IEEE 2000 International Geoscience and Remote Sensing Sym posium (IGARSS'00). Honolulu, HI: IEEE, 5: 1857–1859

Moore S E, Lien R-C. 2007. Pilot whales follow internal solitary waves in the South China Sea. Marine Mammal Science, 23(1): 193–196

Moum J N, Klymak J M, Nash J D, et al. 2007. Energy transport by nonlinear internal waves. Journal of Physical Oceanography, 37(7): 1968–1988

Orr M H, Mignerey P C. 2003. Nonlinear internal waves in the South China Sea: Observation of the conversion of depression internal waves to elevation internal waves. Journal of Geophysical Research, 108(C3): 3064

Osborne A R, Burch T L. 1980. Internal solitons in the Andaman Sea. Science, 208(4443): 451–460

Ramp S R, Tang T Y, Duda T F, et al. 2004. Internal solitons in the northeastern South China Sea. Part I: Sources and deep water propagation. IEEE Journal of Oceanic Engineering, 29(4): 1157–1181

St Laurent L, Simmons H, Tang T Y, et al. 2011. Turbulent properties of internal waves in the South China Sea. Oceanography, 24(4): 78–87

Stanton T P, Ostrovsky L A. 1998. Observations of highly nonlinear internal solitons over the continental shelf. Geophys Res Lett, 25(14): 2695–2698

Yang Y J, Fang Y C, Chang M-H, et al. 2009. Observations of second baroclinic mode internal solitary waves on the continental slope of the northern South China Sea. J Geophys Res, 114(C10): C10003

Yang Y J, Fang Y C, Tang T Y, et al. 2010. Convex and concave types of second baroclinic mode internal solitary waves. Nonlinear Pro-

cesses in Geophysics, 17(6): 605–614

Zhao Zhongxiang, Klemas V, Zheng Quanan, et al. 2004. Remote sensing evidence for baroclinic tide origin of internal solitary waves in the northeastern South China Sea. Geophys Res Lett, 31(6): L06302

Zhao Zhongxiang, Klemas V V, Zheng Quanan, et al. 2003. Satellite observation of internal solitary waves converting polarity. Geophysical Research Letters, 30(19): 1988